Physical Layer Abstraction Model for RadioWeaves

Rimalapudi Sarvendranath, Unnikrishnan Kunnath Ganesan, Zakir Hussain Shaik, and Erik G. Larsson
Department of Electrical Engineering (ISY), Linköping University, Linköping, Sweden - 581 83.
Email: {sarvendranath.rimalapudi, unnikrishnan.kunnath.ganesan, zakir.hussain.shaik, erik.g.larsson}@liu.se

***Abstract*—RadioWeaves, in which distributed antennas with integrated radio and compute resources serve a large number of users, is envisioned to provide high data rates in next-generation wireless systems. In this paper, we develop a physical layer abstraction model to evaluate the performance of different RadioWeaves deployment scenarios. This model helps speed up system-level simulators of the RadioWeaves and is made up of two blocks. The first block generates a vector of signal-to-interference-plus-noise ratios (SINRs) corresponding to each coherence block, and the second block predicts the packet error rate corresponding to the SINRs generated. The vector of SINRs generated depends on different parameters such as the number of users, user locations, antenna configurations, and precoders. We have also considered different antenna gain patterns, such as omni-directional and directional microstrip patch antennas. Our model exploits the benefits of exponential effective SINR mapping (EESM). We study the robustness and accuracy of the EESM for RadioWeaves.**

***Index Terms*—RadioWeaves, beyond 5G, cell-free, physical-layer-abstraction, EESM.**

I. Introduction

RadioWeaves is an emerging physical-layer wireless access infrastructure, in which a fabric of distributed radio devices and computing resources serve as a massive distributed antenna array [1], [2]. The technology builds upon the foundations of massive multiple input multiple output (MIMO) and combines the advantages of the distributed cell-free architectures and the large intelligent surfaces to achieve superior coverage at low power consumption. RadioWeaves enables new, innovative use cases ranging from robotized factories, warehouses, immersive entertainment, and assisted living to smart homes. RadioWeaves is foreseen to be a fundamental enabler of future 6G and beyond networks, which will offer consistent service and scalable network capacity at unprecedented energy efficiency.

Antennas in RadioWeaves can be arranged different topologies, either in a linear topology (for instance, "radio stripe") or in a mesh topology. In terms of spatial signal processing, RadioWeaves inherits the fundamental advantages of cellular massive MIMO: operation time-division duplexing (TDD), reliance on uplink pilots for all channel estimation tasks, and fully digital radio-frequency (RF) processing per antenna. Beyond this, there are many other benefits [2]. First, with increased spatial diversity, a terminal is likely to be close to at least a handful of antennas. This yields a superior degree of macro-diversity against signal blockage, and provides favorable path loss conditions. Second, the angular directions to the service antennas that are visible from a terminal will typically span a broad range, which causes favorable propagation conditions for the transmission of multiple data streams. The RadioWeaves distributed infrastructure has been shown to achieve many orders of magnitude improvements in quality-of-service and energy efficiency, compared to a conventional collocated MIMO system [1].

This work was funded by the REINDEER project of the European Union's Horizon 2020 research and innovation program under grant agreement No. 101013425.

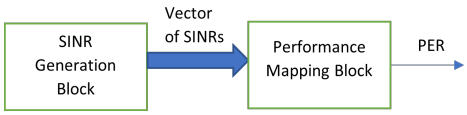

Fig. 1: Physical-layer abstraction model for RadioWeaves

Evaluation of the physical layer performance of this new RadioWeaves infrastructure is important. In this paper, we develop an effective signal-to-interference-plus-noise ratio (SINR) based physical-layer abstraction model to evaluate the performance of a RadioWeaves system. This abstraction model helps to avoid computationally expensive physical-layer link-level simulations and predicts performance with high accuracy. For this reason, it is routinely used for system-level simulation of many wireless standards such as LTE [3], [4], WiMAX [5] and 5G-NR [6]. As shown in Fig. 1, the physical-layer abstraction model is made up of following two blocks.

1) *SINR Generation Block:* The first block calculates a vector of SINRs per user for each coherence block, where the channel remains unchanged.
2) *Performance Mapping Block:* The second block takes the vector of SINRs from SINR Generation Block and predicts the instantaneous packet error rate (PER) based on the modulation and coding scheme (MCS) used for the transmission.

This performance mapping block first maps the vector of SINRs onto a scalar called the effective SINR. In the literature, different mappings are considered to map vector of SINRs to effective SINR. For example, in *average value interface [7]*, the effective SINR is the arithmetic average of the vector of SINRs. This is generally used to model flat-fading channels and is not an accurate measure for frequency selective channels [7]. It is also independent of the MCS used. In *capacity based mapping* [7], [8], the additive white Gaussian noise (AWGN) channel capacity formula is used as the mapping function. Here, the high SINR values impact the effective SINR more than the low SINR values as the mapping

function increases monotonically. This makes the capacity-based mapping inaccurate as the PER is mostly impacted by the low SINR values [4].

In this paper, we study the exponential effective SINR mapping (EESM) mapping, which is obtained by generalizing the PER of an uncoded BPSK transmission over an AWGN channel [7], [9]. The generalization is done by introducing an MCS-dependent parameter. We focus on EESM as it has been shown to achieve a good trade-off between accuracy and computational complexity. It is also shown to be applicable in systems with inter-cell interference [5], [10] and to OFDM systems with HARQ [11]. Furthermore, EESM has been validated to perform accurately for several wireless standards. It is shown to predict the performance accurately for MCS employed in IEEE 802.16 WiMAX [12], LTE [3], [4] and 5G NR [6].

In this paper, we develop an EESM based abstraction model for the RadioWeaves. We present the distribution of SINRs for different RadioWeaves scenarios under different precoders such as zero forcing and maximum ratio. We also compare their behavior with perfect and imperfect channel state information (CSI) and different antenna gain patterns. We also validate the robustness of the EESM parameter calibration for different scenarios including extreme SINR profiles.

Outline: Our system model is introduced in Section II. SINR generation block is described in Section III. Section IV describes the performance mapping block and robustness of calibration. Our main conclusions are summarized in Section V.

The following notation is used in the sequel. Boldface lowercase letters, $\mathbf{a}$, denote column vectors and boldface uppercase letters, $\mathbf{A}$, denote matrices. The superscripts $(\cdot)^*$, $(\cdot)^T$, and $(\cdot)^H$ denote the conjugate, transpose, and Hermitian transpose, respectively. The notation $\mathbf{I}_N$ represents the $N \times N$ identity matrix. The (m,n)th element of a matrix $\mathbf{A}$ is denoted by $[\mathbf{A}]_{mn}$. The absolute value of a scalar and l_2-norm of a vector are denoted by $|\cdot|$ and $\|\cdot\|$, respectively. We use $\mathbf{z} \sim \mathcal{CN}(\mathbf{0}, \mathbf{C})$ to denote a multi-variate circularly symmetric complex Gaussian random vector with zero mean and covariance matrix $\mathbf{C}$.

II. System Model

We consider a RadioWeaves system, where M antennas connected to a central processing unit (CPU) jointly serve K single antenna users. Let $g_{mk} \in \mathbb{C}$ denote the complex channel gain from m^{th} transmit antenna to the k^{th} user located at $(r_{mk}, \theta_{mk}, \varphi_{mk})$ in the spherical coordinate system. Let $\mathbf{G} = [g_{mk}] \in \mathbb{C}^{M \times K}$ be the channel matrix between the M transmit antennas and the K users. We assume that the service antennas are spaced apart that coupling is insignificant.

1) Uplink: In the uplink, all the users coherently transmit data to the base station. The collective signal received at the service antennas, $\mathbf{y}_{\text{ul}} \in \mathbb{C}^{M \times 1}$, is

$$\mathbf{y}_{\text{ul}} = \sqrt{\rho_{\text{ul}}}\mathbf{G}\mathbf{D}\mathbf{q} + \mathbf{w}_{\text{ul}}, \tag{1}$$

where ρ_{ul} is the uplink transmit power, $\mathbf{D}$ is a diagonal matrix of power control coefficients $\text{diag}\{\sqrt{\eta_1}, \ldots, \sqrt{\eta_k}\}$, $0 \leq \eta_k \leq 1$ is the power control coefficient of k^{th} user, $\mathbf{q} \in \mathbb{C}^{K \times 1}$ is the data from all users, and $\mathbf{w}_{\text{ul}} \sim \mathcal{CN}(0, N_0\mathbf{I}_M)$ is the noise and N_0 is the noise power spectral density.

2) Downlink: In the downlink, the service antennas jointly transmit the data $\mathbf{q} \in \mathbb{C}^{K \times 1}$ such that $\mathbb{E}\{\|\mathbf{q}\|^2\} \leq 1$ to all the users. The collective signal received at the users IS denoted by the vector $\mathbf{y}_{\text{dl}} \in \mathbb{C}^{K \times 1}$ and is expressed as

$$\mathbf{y}_{\text{dl}} = \sqrt{\rho_{\text{dl}}}\mathbf{G}^{\text{H}}\mathbf{A}\mathbf{D}\mathbf{q} + \mathbf{w}_{\text{dl}}, \tag{2}$$

where ρ_{dl} is the downlink transmit power and $\mathbf{A} \in \mathbb{C}^{M \times K}$ is the precoding matrix to spread the K signals into M antennas. Here, the power control coefficients are chosen such that $\sum_{k=1}^{K} \eta_k \leq 1$ and $\mathbf{w}_{\text{dl}} \sim \mathcal{CN}(0, N_0\mathbf{I}_K)$ is the noise.

A. Channel Models

We consider two channel models: i) Line-of-sight and ii) independent Rayleigh fading.

1) Line-of-Sight: First, a line-of-sight channel for a free-space signal propagation environment is modeled. Assuming an omni-directional antenna at the user, the received power can be written as

$$P_{rx} = \frac{P_{rad}}{4\pi}\, G(\theta, \varphi)\, \frac{1}{r^2}\, \frac{\lambda^2}{4\pi}. \tag{3}$$

where $G(\theta, \varphi)$ is the directional power gain of the transmit antenna, P_{rad} is the transmitted radiated power, r is the distance between the transmitter and the receiver and λ is the wavelength of the transmitted signal.

2) Independent Rayleigh Fading: In a rich scattering environment, we consider the channel to be Rayleigh distributed with independent fading across antennas. Each channel gain g_{mk} is distributed as $\mathcal{CN}(0, \beta_{mk})$, where β_{mk} is the large scale path loss fading coefficient between transmitter and receiver with distance d_{mk}. It is modeled as $\beta_{mk} = -30.5 - 36.7 \log_{10}(d_{mk}/1\text{m})$ dB [13].

B. Antenna Gain Pattern

We consider two antenna gain patterns: (i) Omni-directional and (ii) Rectangular microstrip patch antennas. Gain pattern of the omni-directional antenna is independent of the angles θ and φ, i.e., $G(\theta, \varphi) = 1$. The gain pattern of the rectangular microstrip patch antenna is given by

$$G(\theta, \varphi) = \left(\alpha \sin(\theta) \frac{\sin(X)}{X} \frac{\sin(Z)}{Z}\right)^2, \tag{4}$$

where

$$X = \frac{\pi h}{\lambda} \sin(\theta)\cos(\varphi), \tag{5}$$

$$Z = \frac{\pi W}{\lambda} \cos(\theta), \tag{6}$$

$$\alpha^2 = \frac{4\pi}{\displaystyle\int_{\theta=0}^{\pi} \int_{\varphi=-\frac{\pi}{2}}^{\frac{\pi}{2}} \left(\frac{\sin(X)}{X} \frac{\sin(Z)}{Z}\right)^2 \sin^3(\theta) d\theta d\varphi}. \tag{7}$$

and h and W denote the height and width, respectively, of the patch antenna [14, Ch. 14]. With vertical polarization and with no polarization losses the complex channel gain g_{mk} for a microstrip patch antenna is given by [14],

$$g_{mk} = \frac{\alpha\lambda}{4\pi r} e^{-j\frac{2\pi r}{\lambda}} \sin(\theta) \frac{\sin(X)}{X} \frac{\sin(Z)}{Z}. \tag{8}$$

C. Channel Estimation

We consider least-squares (LS) channel estimation. Let τ_c denote the length of the coherence interval (see, e.g., Chapter 2 of [15]) and we assume there are τ_p mutually orthogonal pilot sequences of length $\tau_c \geq \tau_p \geq K$. Let $\boldsymbol{\phi}_k \in \mathbb{C}^{\tau_p \times 1}$ be the pilot sequence associated with user k, which is the k^{th} column of the $\tau_p \times K$ unitary matrix $\boldsymbol{\Phi}$ and $\boldsymbol{\Phi}^H\boldsymbol{\Phi} = \mathbf{I}_K$. Each user transmits $\sqrt{\tau_p}\boldsymbol{\phi}_k^H$ over τ_p symbols and the signals collectively received $\mathbf{Y}_p \in \mathbb{C}^{M\times\tau_p}$ can be written as $\mathbf{Y}_p = \sqrt{\rho_{\text{ul}}\tau_p}\mathbf{G}\boldsymbol{\Phi}^H + \mathbf{W}_p$, where $\mathbf{W}_p$ is the noise matrix with i.i.d $\mathcal{CN}(0,\sigma^2)$ elements. De-spreading operation is performed on the received signal $\mathbf{Y}_p$ and is given by

$$\mathbf{Y}'_p = \mathbf{Y}_p\boldsymbol{\Phi} = \sqrt{\rho_{\text{ul}}\tau_p}\mathbf{G} + \mathbf{W}_p\boldsymbol{\Phi}. \tag{9}$$

Let $\hat{g}_{mk}$ denote the LS channel estimate of g_{mk}. It is given by

$$\hat{g}_{mk} = [\mathbf{Y}'_p]_{mk}/\sqrt{\rho_{\text{ul}}\tau_p}. \tag{10}$$

Let $\hat{\mathbf{G}} \in \mathbb{C}^{M\times K}$ denote the estimated channel matrix and let $\hat{\mathbf{g}}_k = [\hat{g}_{1k},\ldots,\hat{g}_{Mk}]^T$ is the estimated channel vector corresponding to the k^{th} user.

D. Precoding/Combiners

In uplink, we consider the most commonly employed receiver combiners, maximum-ratio combining (MRC) and zero-forcing (ZF). The MRC matrix is given by $\mathbf{V}^{\text{MRT}} = [\mathbf{v}_1^{\text{MRT}},\ldots,\mathbf{v}_K^{\text{MRT}}]^H$, where $\mathbf{v}_k^{\text{MRT}} = \hat{\mathbf{g}}_k/\|\hat{\mathbf{g}}_k\|$. The ZF receiver matrix is given by $\mathbf{V}^{\text{ZF}} = \left(\hat{\mathbf{G}}^H\hat{\mathbf{G}}\right)^{-1}\hat{\mathbf{G}}^H$

In downlink, we consider most commonly used precoders such as maximum-ratio transmission (MRT) and ZF. The MRT matrix defined by $\mathbf{A}^{\text{MRT}} = [\mathbf{a}_1^{\text{MRT}},\ldots,\mathbf{a}_K^{\text{MRT}}]$, where $\mathbf{a}_k^{\text{MRT}} = \hat{\mathbf{g}}_k/\|\hat{\mathbf{g}}_k\|$. The ZF precoder is given by $\mathbf{A}^{\text{ZF}} = \hat{\mathbf{G}}^H\left(\hat{\mathbf{G}}\hat{\mathbf{G}}^H\right)^{-1}$. Note that in the next section, we will use the notation $\mathbf{a}_k$ and $\mathbf{v}_k$ for downlink precoder and uplink combiner, respectively, to account for both maximum-ratio and zero-forcing.

III. SINR Generation

The first block of the abstraction model shown in Fig. 1 generates one SINR value per coherence block for given user based on the channel model (coherence time, coherence bandwidth) and other parameters (carrier frequency and bandwidth). The block also takes as input the number of users, user locations, number of antennas, antenna gain patterns, antenna configurations, channel estimator, precoder and combiner, pilot, and noise power. Therefore, the resulting vector of SINRs depends on depends on different parameters, including large and small scale fading. Here, we outline the SINR computation for both uplink and downlink scenarios.

Table I: Simulation Parameters for SINR analysis

Frequency of operation, f	2 GHz
Antenna Deployment	ULA over four walls
Signal bandwidth	20 MHz
Subcarrier bandwidth	200 kHz
Mobility	Static
Base station power	1 mW
Base station noise figure	5 dB
User power	1 μW
Pilot power	20 μW
User noise figure	9 dB
Channel type	LOS
Dielectric constant, ε_r	10.2
Height of patch antenna, h	0.1588 cm
Temperature of Operation	300 K

1) Downlink: In a coherence block, the collective signal received at all the users is given by

$$\mathbf{y}_{\text{dl}} = \sqrt{\rho_{\text{dl}}}\mathbf{G}^{\text{H}}\mathbf{A}\mathbf{D}\mathbf{q} + \mathbf{w}. \tag{11}$$

Thus at each user, the received signal can be written as

$$y_k = \sqrt{\rho_{\text{dl}}}\mathbf{g}_k^{\text{H}}\mathbf{A}\mathbf{D}\mathbf{q} + w_k \tag{12}$$

$$= \sqrt{\rho_{\text{dl}}\eta_k}\mathbf{g}_k^{\text{H}}\mathbf{a}_k q_k + \sum_{i=1,i\neq k}^{K}\sqrt{\rho_{\text{dl}}\eta_i}\mathbf{g}_k^{\text{H}}\mathbf{a}_i q_i + w_k. \tag{13}$$

The instantaneous SINR at user k, is then given by

$$\text{SINR}_k^{\text{inst.}} = \frac{\rho_{\text{dl}}\eta_k|\mathbf{g}_k^{\text{H}}\mathbf{a}_k|^2}{\sum_{i=1,i\neq k}^{K}\rho_{\text{dl}}\eta_i|\mathbf{g}_k^{\text{H}}\mathbf{a}_i|^2 + \sigma^2}, \tag{14}$$

where noise power $\sigma^2 = k_B \cdot T \cdot BW \cdot 10^{-\text{NF}/10}$ and $k_B = 1.23\times10^{-23}JK^{-1}$ is the Boltzmann constant, T (in Kelvin) is the temperature, BW (in Hertz) is the bandwidth under consideration, and NF is the noise figure in dB. At this, we remark that for this instantaneous SINR to have a rigorous information-theoretic operational meaning, each UE needs to know the instantaneous value of $\mathbf{g}_k^{\text{H}}\mathbf{a}_k$ as well as the instantaneous SINR. These can be estimated to a good degree of accuracy by using techniques from for example [16] and for the purpose of obtaining an approximate performance prediction we will here assume that they are known.

Figs. 2 and 3 show the cumulative distribution function (CDF) of the downlink SINR in a RadioWeave deployment in two different scenarios. The simulation setup is provided in Table I. From the figure, it can be seen that ZF performs much better than MRT as ZF can suppress interference from other users. Moreover, the ZF significantly outperforms MRT under imperfect CSI scenarios. The gain from the patch antennas can be exploited well by the ZF approach, while MRT is not able to exploit the antenna gain as the interference term dominates. The randomness in this simulation is due to the random spatial distribution of the users, the channel estimation errors, and variations of the channel response among the subcarriers. An important observation is that the CDFs are very stable, that is, the probability of having a scenario (in terms of coordinates of the users) or seeing a channel realization that result in poor performance is miniscule.

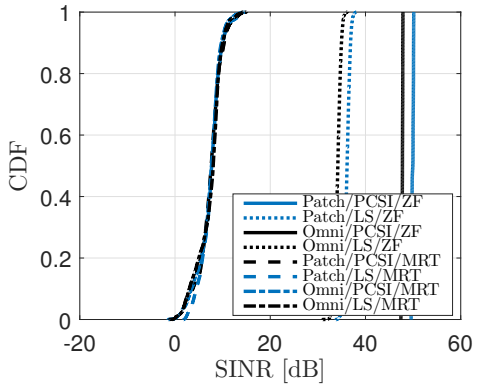

Fig. 2: Downlink SINR for a room with 40mx40mx10m size, $M = 512$, and $K = 100$. The legend is to be read as antenna type/estimation method/precoder

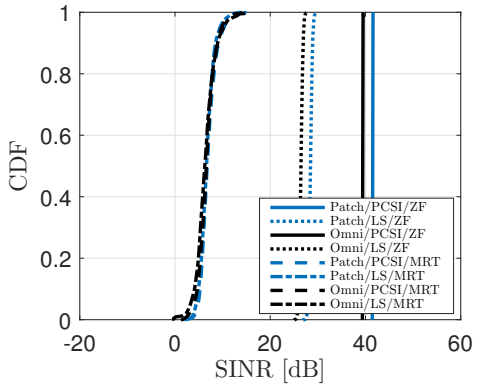

Fig. 3: Downlink SINR for a room with 140mx70mx15m room size (the production hall in [17, p. 46]), $M = 1024$, $K = 200$.

2) Uplink: The collective signal received from all the users at the CPU is given by

$$\mathbf{y}_{\text{ul}} = \sqrt{\rho_{\text{ul}}}\mathbf{G}\mathbf{D}\mathbf{q} + \mathbf{w}. \tag{15}$$

We perform a combining operation by a matrix $\mathbf{V} \in \mathbb{C}^{K\times M}$ at the CPU, given by

$$\mathbf{V}\mathbf{y}_{\text{ul}} = \sqrt{\rho_{\text{ul}}}\mathbf{V}\mathbf{G}\mathbf{D}\mathbf{q} + \mathbf{V}\mathbf{w}. \tag{16}$$

Thus the decision statistic of user k is given by

$$\mathbf{v}_k^{\text{H}}\mathbf{y}_{\text{ul}} = \sqrt{\rho_{\text{ul}}}\mathbf{v}_k^{\text{H}}\mathbf{G}\mathbf{D}\mathbf{q} + \mathbf{v}_k^{\text{H}}\mathbf{w} \tag{17}$$

$$= \sqrt{\rho_{\text{ul}}\eta_k}\mathbf{v}_k^{\text{H}}\mathbf{g}_k q_k + \sum_{i=1,i\neq k}^{K} \sqrt{\rho_{\text{ul}}\eta_i}\mathbf{v}_k^{\text{H}}\mathbf{g}_i q_i + \mathbf{v}_k^{\text{H}}\mathbf{w}. \tag{18}$$

As the combining vector $\mathbf{v}_k$ is unit-norm, the instantaneous SINR at user k at the CPU is

$$\text{SINR}_k^{\text{inst.}} = \frac{\rho_{\text{ul}}\eta_k|\mathbf{v}_k^{\text{H}}\mathbf{g}_k|^2}{\sum_{i=1,i\neq k}^{K}\rho_{\text{ul}}\eta_i|\mathbf{v}_k^{\text{H}}\mathbf{g}_i|^2 + \sigma^2}. \tag{19}$$

Fig. 4 shows the CDF of uplink SINR for a RadioWeave deployment. We see similar behavior as in the downlink case.

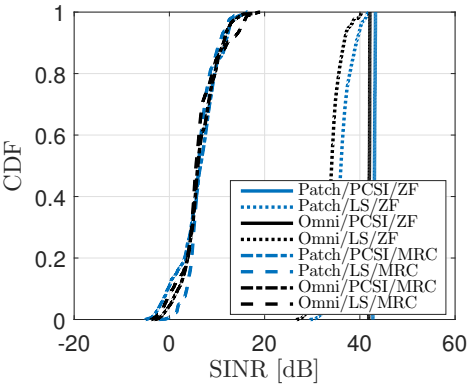

Fig. 4: Uplink SINR for a room with 40mx40mx10m size, $M = 512$, $K = 100$.

Fig. 5: Performance Mapping Block

For ZF, we see that the range of SINR variations similar to the downlink secnario in Fig. 2. However, the variation is higher for MRC.

IV. Performance Mapping

We now describe the second block of the abstraction model. As explained earlier, the performance mapping accurately predicts the link-level performance in a computationally efficient manner. It helps to speed up the system-level simulations as well. The performance mapping block contains two stages, namely, *SINR compression* and *quality mapping* as shown in Fig. 5. The SINR compression block takes in a vector of SINRs and outputs a scalar, which is known as effective SINR. The quality mapping block maps this effective SINR to the PER. To understand the accuracy of the mapping, its predicted performance is compared with actual performance obtained through link-level simulations. We focus on EESM, which is shown to be accurate and has a computationally simple form.

A. SINR Compression

The compression of the vector of SINRs onto the effective SINR combines all the different SINRs seen by the block of data into a single scalar number as each SINRs corresponds to different coherence blocks over which data is encoded. Specifically, this models the link as an equivalent AWGN channel and the effective SINR can be interpreted as the equivalent signal-to-noise-ratio (SNR) on an AWGN channel. This compression in general depends on the MCS employed, and predicts the performance in a computationally efficient manner.

Let $\gamma = [\gamma_1, \ldots, \gamma_N]^T$ denote the vector of SINRs and γ_{eff} denote the effective SINR. Then, the general form of compression is given by [5], [7]

$$\gamma_{\text{eff}} = \beta f^{-1}\left(\frac{1}{N}\sum_{n=1}^{N} f\left(\frac{\gamma_n}{\beta}\right)\right), \tag{20}$$

where $f(\cdot)$ is a function used to compress [7] and β is an MCS-dependent parameter. This parameter β should be calibrated empirically to achieve accurate prediction. The accuracy of this compression is, as it turns out, very robust and a value of β optimized for one scenario can also be used in many other, quite different scenarios. We further elaborate on this in Section IV-B. However, importantly, each MCS has a different associated β.

For EESM, $f(\gamma_n) = 1 - \exp(-\gamma_n)$ [7], [18], [19]. Therefore, the effective SINR is given by

$$\gamma_{\text{eff}} = -\beta \log\left(\frac{1}{N}\sum_{n=1}^{N} \exp\left(-\frac{\gamma_n}{\beta}\right)\right). \tag{21}$$

The emphasis given to lower SINR values allows it to accurately predict the PER.

B. Quality Mapping

The effective SINR computed by SINR compression block is mapped to PER. Link-level simulations of the RadioWeaves are performed initially to calibrate this quality mapping block. Once calibration has been performed, the computationally intensive link-level simulations need not be performed again. For calibration of β, we have used the procedure described in [20, Ch. 3.2.2]. This calibration is performed only once for an MCS and the optimal β^* is stored in a lookup table. Table II and Table III show the calibrated values of β^* for RadioWeaves for different MCS with LDPC and polar coding, respectively. With polar coding, cyclic redundancy check (CRC) bits, interleaving and rate matching are taken into consideration.

Table II: Calibrated β^* values for RadioWeaves with LDPC codes

MCS index	Modulation	Code rate	β^*
0	BPSK	1/2	0.78
1	QPSK	1/2	1.55
2	16-QAM	1/2	4.16

Table III: Calibrated β^* values for RadioWeaves with polar codes

MCS index	Modulation	Code rate	β^*
1	QPSK	1/2	0.624

Fig. 6 plots the effective SINR $\gamma_{\text{eff}}(\beta^*)$ on the horizontal axis and the simulated PER of RadioWeaves on the vertical axis (shown in red markers) for different realizations of the vector of SINRs. This is done for different MCS with LDPC codes. The calibrated β values for different MCSs, which are tabulated in Table II, are used in generating the plot. We note

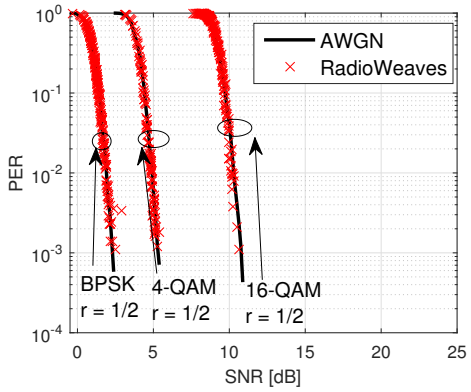

Fig. 6: Validation of EESM: Performance of RadioWeaves as a function of effective SINR.

Table IV: Calibrated β^* values for different parameter values (MCS index =1)

Number of antennas	Number of subcarriers	β^*
48	2	1.54
48	18	1.55
64	2	1.54
64	18	1.55

that the markers represent the actual PER of the RadioWeaves system obtained through link-level simulations. They are plotted against the effective SINR obtained through the EESM mapping with calibrated β^*. Also, shown is the PER curve of AWGN channel with SNR equal to the effective SINR, and for the same choices of MCS. We see that the markers, which represent the actual performance of the RadioWeaves system, match well with the AWGN PER values, which represent the predicted values. This establishes that the prediction accuracy of EESM is very good.

Robustness of β: To verify the robustness of the calibration parameter β, for a given MCS, we repeated the calibration with different values of antenna elements and subcarriers. Table IV shows the calibrated β values with different parameters. It clearly shows that the variation in the value of β is negligible. This is in line with the conclusions in [6], where the variation in β^* values is shown to be negligible as the subcarrier spacing or other 5G-NR numerology changes.

Furthermore, in Table V, we compared the simulated PER and the predicted PER for different parameters values for which calibration is not performed. Here, the simulated PER is obtained through the RadioWeaves link-level simulations and the predicted PER is obtained by the EESM-based performance mapping. It also compares the simulated PER with predicted PER for two values of β^* from Table IV. We see that the predicted values are very close to the simulated and they change only by a small value as β^* varies slightly.

Extreme SINR profile: We now consider an extreme, artificial example in order to demonstrate the robustness of the EESM technique. We specifically study the behavior of the performance mapping for an SINR profile that is not used for calibration of β. This SINR profile has a set of SINR values

Table V: Comparison of simulated PER with predicted PER for different values of β^* (M=72, QPSK, and rate=0.5)

Simulated PER	Predicted PER (β^*=1.54)	Predicted PER (β^*=1.6)
0.0027	0.0039	0.0038
0.0015	0.0009	0.0009
0.0008	0.0006	0.0005
0.5040	0.4849	0.4830
0.2920	0.3081	0.3059
0.2760	0.2714	0.2693

Table VI: Comparison of simulated PER with predicted PER for extreme SINR profile shown in Figure 7 for M=72, QPSK, and rate=0.5.

Simulated PER	Predicted PER (β^*=1.54)
0.0187	0.0173
0.0251	0.0254
0.0256	0.0199
0.0222	0.0188
0.0255	0.0212
0.0145	0.0163
0.0138	0.0156
0.0118	0.0162

that are extremely low, as shown in Fig. 7. Table VI compares the simulated PER with the predicted PER for $\beta^* = 1.54$. We see that the predicted PERs are reasonably close to the simulated PER values even for this extreme SINR profile for which calibration is not done.

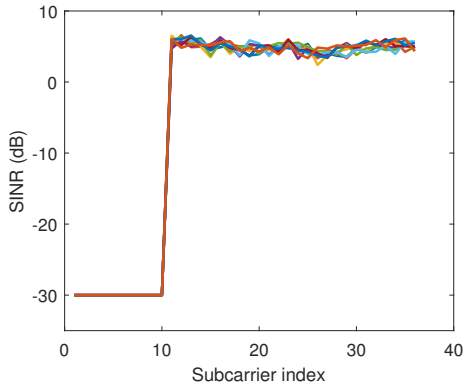

Fig. 7: Extreme SINR profile as a function of subcarrier index. Here, different curves correspond to different realizations for which PER's are shown in Table VI.

V. Conclusion

We presented a physical-layer abstraction model for the RadioWeaves infrastructure. This model enables the prediction of the RadioWeaves physical layer performance in a computationally efficient manner with high accuracy. It can especially be used to speed up system-level simulations of RadioWeaves. Our simulations showed that EESM performs well for different MCSs. The study has also shown that the calibration parameter is mainly dependent on the MCS used and that once it is obtained for a particular MCS, it can be used across a wide range of scenarios with different parameters such as the number of antennas and the number of subcarriers. We showed that the EESM is a highly robust way of mapping a vector of instantaneous SINRs to link-level performance in terms of PERs for a variety of scenarios, where calibration is required only once and where the specific scenario selected for the calibration is not particular important.

References

[1] U. K. Ganesan, E. Björnson, and E. G. Larsson, "RadioWeaves for extreme spatial multiplexing in indoor environments," in *54th Asilomar Conference on Signals, Systems, and Computers*. IEEE, 2020.

[2] L. Van der Perre, E. G. Larsson, F. Tufvesson, L. De Strycker, E. Björnson, and O. Edfors, "RadioWeaves for efficient connectivity: analysis and impact of constraints in actual deployments," in *53rd Asilomar Conference on Signals, Systems, and Computers*. IEEE, 2019, pp. 15–22.

[3] J. Fan, Q. Yin, G. Y. Li, B. Peng, and X. Zhu, "MCS selection for throughput improvement in downlink LTE systems," in *Proc. ICCCN*, Aug. 2011, pp. 1–5.

[4] R. Jain, C. So-In, and A. K. A. Tamimi, "System-level modeling of IEEE 802.16e mobile WiMAX networks: Key issues," *IEEE Wireless Commun.*, vol. 15, no. 5, pp. 73–79, Oct. 2008.

[5] R. Srinivasan, J. Zhuang, L. Jalloul, R. Novak, and J. Park, "IEEE 802.16m evaluation methodology document (EMD)," Tech. Rep. IEEE 802.16m-08/004r2, 2008.

[6] S. Lagen, K. Wanuga, H. Elkotby, S. Goyal, N. Patriciello, and L. Giupponi, "New radio physical layer abstraction for system-level simulations of 5G networks," in *IEEE International Conference on Communications (ICC)*, Jun. 2020, pp. 1–7.

[7] S. S. Tsai and A. C. K. Soong, "Effective-SNR mapping for modeling frame error rates in multiple-state channels," 3GPP2, Tech. Rep. 3GPP2-C30-20030429-010, 2003.

[8] J. Kim, A. Ashikhmin, A. J. van Wijngaarden, E. Soljanin, and N. Gopalakrishnan, "On efficient link error prediction based on convex metrics," in *Proc. VTC (Fall)*, Sep. 2004, pp. 4190–4194.

[9] E. Westman, "Calibration and evaluation of the exponential effective SINR mapping (EESM) in 802.16," Master's thesis, The Royal Institute of Technology (KTH), Stockholm, Sweden, Sep. 2006.

[10] E. M. G. Stancanelli, F. R. P. Cavalcanti, and Y. C. B. Silva, "Revisiting the effective SINR mapping interface for link and system level simulations of wireless communication systems," in *Proc. LatinCOM*, Oct. 2011, pp. 1–6.

[11] B. Classon, P. Sartori, Y. Blankenship, K. Baum, R. Love, and Y. Sun, "Efficient OFDM-HARQ system evaluation using a recursive EESM link error prediction," in *Proc. WCNC*, Apr. 2006, pp. 1860–1865.

[12] "Air interface for fixed broadband wireless access systems," IEEE Standard for local and Metropolitan Area Networks, Tech. Rep. IEEE 802.16-2004, Part 16, Oct. 2004.

[13] E. Björnson and L. Sanguinetti, "Making cell-free massive MIMO competitive with MMSE processing and centralized implementation," *IEEE Transactions on Wireless Communications*, vol. 19, no. 1, pp. 77–90, 2019.

[14] C. A. Balanis, *Antenna Theory: Analysis and Design*. John Wiley & sons, 2016.

[15] T. L. Marzetta, E. G. Larsson, H. Yang, and H. Q. Ngo, *Fundamentals of Massive MIMO*. Cambridge University Press, 2016.

[16] G. Interdonato, H. Q. Ngo, P. Frenger, and E. G. Larsson, "Downlink training in cell-free massive MIMO: A blessing in disguise," *IEEE Transactions on Wireless Communications*, vol. 18, no. 11, pp. 5153–5169, 2019.

[17] H2020 REINDEER D1.1, "Use case-driven specifications and technical requirements and initial channel model," Tech. Rep. DOI: 10.5281/zenodo.5561844, 2021.

[18] Ericsson, "System-level evaluation of OFDM – further considerations," TSG-RAN WG1 #35, Tech. Rep. R1-031303, 2003.

[19] A. Karim, "Exponential effective signal to noise ratio mapping (EESM) computation for WiMAX physical layer," Master's thesis, Washington Univ., May 2007.

[20] J. Francis, "Wideband rate adaptation and scheduling in ofdm cellular systems: Modeling, analysis, and base station-side estimation," Ph.D. dissertation, Indian Institute of Science, Bangalore, Aug. 2017.